Structural Evolution of Complexes of Poly(styrenesulfonate) and Cetyltrimethylammonium Chloride

Richard G. Nause,[†] David A. Hoagland,[†] and Helmut H. Strey*[,‡]

Department of Polymer Science and Engineering, University of Massachusetts, Amherst, Massachusetts 01003, and Department of Biomedical Engineering, Stony Brook University, Stony Brook, New York 11790

Received July 23, 2007; Revised Manuscript Received March 20, 2008

ABSTRACT: Structural evolution is tracked as a charged surfactant, cetyltrimethylammonium chloride (CTAC), is titrated into a solution of oppositely charged polyelectrolyte, sodium poly(styrenesulfonate), to form polyelectrolyte−surfactant complexes. At surfactant-to-polymer molar charge ratio [*r*] less than 0.5, small-angle neutron scattering of the soluble complexes reveals bound spherical CTAC micelles of radii 21−24 Å, slightly less than for pure CTAC. At such small [*r*], the number of spherical micelles per chain grows with [*r*] but never becomes large (<2). At [*r*] ∼ 0.5, if salt concentration is low (<100 mM), cylindrical micelles of radii 20−22 Å and aspect ratio at least 5:1 replace the spherical micelles. Irrespective of salt concentration, at [*r*] ∼ 0.7 precipitation occurs, with X-ray scattering revealing CTAC arranged into hexagonally close-packed cylinders. At even higher [*r*], the hexagonal phase transforms into the *Pm*3*n* cubic phase. Raising ionic strength diminishes NaPSS−CTAC attraction, delaying onset of insolubility and disrupting precipitate order.

Introduction

Structural investigation of polymer−surfactant complexes first focused on complexes of neutral polymer and anionic surfactant. Small-angle neutron scattering (SANS) showed that the complexed surfactants organize into roughly spherical micelles spaced along the backbones of isolated polyelectrolyte chains,[1–4] a motif described as the "pearl necklace".[1–7] Because of surfactant charge, such soluble complexes display some behaviors typical of polyelectrolytes. Complexes of neutral polymer and charged surfactant remain soluble regardless of the relative concentrations of the two components.

In contrast, because of stronger polymer−surfactant attractions, the bulk ratio [*r*] of surfactant-to-polyelectrolyte molar charge plays a dominant role in polyelectrolyte−surfactant complexes, and above a characteristic order unity value of [*r*], the complexes phase separate into a multiphase liquid coacervate or a solid precipitate. Precipitated polyelectrolyte−surfactant complexes can be highly ordered, not just with soluble polyelectrolyte[8–11] but also with cross-linked polyelectrolyte gels.[12–15] Previous work on stoichiometric ([*r*] = 1) polyelectrolyte−surfactant complexes has shed light on factors contributing to complex morphology, including surfactant tail length,[9,12] polyelectrolyte charge density,[16,17] and degree of hydrophobic modification to polyelectrolyte.[18,19] Few studies have considered the structural evolution with increasing [*r*] as soluble, isolated complexes transform into insoluble, highly ordered complexes.[20–26]

Insoluble polyelectrolyte−surfactant complexes display a myriad of structures, derived mainly from the nature of the surfactant. For a pure surfactant solution, hydrophobic tail length, number of tails, and hydrophilic head-group size principally determine the micelle structure at and somewhat above the critical micelle concentration (cmc).[27] Hydrophobicity brings the tails together, but head-group repulsion prevents gross phase separation. Surfactants with high spontaneous curvature tend to form spherical micelles, while those with lower spontaneous curvatures tend to form cylindrical and laminar micelles. Because spontaneous curvature is governed by intrinsic properties of the surfactant molecule, micelle shape at and near the cmc is difficult to alter,[28,29] but constraining the micelles to small volume offers one possible means. A volume effect is observed when surfactant micelles are packed at high concentrations or placed inside a confinement geometry.[30–32] For the former, a series of morphological transitions occur as concentration increases.[33] For polyelectrolyte−surfactant complexes, each factor listed in the previous paragraph plays an important role. Most importantly, the stronger the interaction between polyelectrolyte and surfactant, the more tightly packed are the micelles.

Assembly of oppositely charged species in aqueous media is by no means a new topic. However, study of the complexes formed between sodium poly(styrenesulfonate) (NaPSS) and quaternary ammonium surfactants, such as cetyltrimethylammoinum chloride (CTAC), has been limited. Aggregation numbers for polyelectrolyte-bound surfactant micelles were estimated using time-resolved fluorescence quenching. At [*r*] = 0.5, Almgren et al.[34] reported an aggregation number of ∼53 for NaPSS−CTAC, a much lower number than for CTAC in absence of NaPSS (90,[30]110,[34] 132[35]). (We will revisit this value in the current report. In fluorescence experiments, NaPSS acts as a quencher, artificially reducing the calculated aggregation number.) Anticipating results of the current investigation, cylindrical micelles were observed for poly(acrylic acid)−cetyltrimethylammonium bromide complexes.[36] Thermodynamic techniques have also been used to study NaPSS−quaternary ammonium surfactant complexes.[1,37]

Light scattering yields the global conformation of a polyelectrolyte−surfactant complex but is incapable of probing its internal structure.[38,39] More suitable methods for elucidation of internal structural are X-ray and neutron scattering, but studies by these methods of NaPSS−quaternary ammonium surfactant systems have been rare. By X-ray scattering, Kogej et al. examined structures formed by NaPSS and *N*-cetyl- or *N*-dodecylpyridinium chloride (CPC and DPC, respectively).[40,41] At [*r*] ∼ 1, they found that CPC organizes into highly ordered hexagonally packaged cylinders, and at [*r*] as low as 0.3, they detected a diffuse Bragg peak. This peak, indicating tight

* Corresponding author: e-mail Helmut.Strey@stonybrook.edu, phone 631-632-1957.
[†] University of Massachusetts.
[‡] Stony Brook University.

10.1021/ma071634u CCC: $40.75
Published on Web 05/07/2008

Table 1. PSS/CTAC SANS Results (10 mM NaCl)

ratio	[PSS] (mM)	[CTAC] (mM)	R (Å)	a (Å)	L (Å)	ν_a	ν_b	N_a	N_b
0.1	12.04	1.204	24.6			109	115	0.46	0.43
0.2	11.98	2.396	25.3	86.3		100	125	1	0.8
0.3	10.52	3.156	25.0	76.7		109	121	1.38	1.24
0.4	17.32	6.93	25.5			130	128	1.54	1.56
0.5	16.17	8.09	19.6*		214	425	474	0.59	0.53
0.6	15.16	9.10	21.3*		220	568	578	0.53	0.52
0.66	14.61	9.64	22.0*		205	510	574	0.65	0.57

Table 2. PSS/CTAC SANS Results (100 mM NaCl)

ratio	[PSS] (mM)	[CTAC] (mM)	R (Å)	a (Å)	L (Å)	ν_a	ν_b	N_a	N_b
0.1	12.04	1.204	24.8			105	118	0.48	0.42
0.2	11.98	2.396	24.7	73.8		97	116	1.03	0.86
0.3	10.52	3.156	24.6	76.3		106	116	1.42	1.29
0.4	17.32	6.93	25.1	67.4		118	122	1.69	1.64
0.5	16.17	8.09	18.9*		>250				
0.6	15.16	9.10	20.1*		>250				
0.66	14.61	9.64	20.3*		>250				

packing of micellar aggregates, demonstrates precipitation at rather low [r]. For [r] above the precipitation point, changes in peak shape and intensity established increasing precipitate accumulation and order. To our knowledge, NaPSS−quaternary ammonium surfactant systems have never been examined by SANS or cryo-TEM.

The NaPSS−CTAC system is considered to be highly interacting due to the strong charging of both polyelectrolyte and surfactant. A complete structural progression for the NaPSS−CTAC system is described here, beginning with no added surfactant and extending well beyond complete neutralization and precipitation. Soluble structures are examined by SANS in D_2O, an approach exploiting the good contrast between micellar cores and surrounding solvent. Previous light scattering experiments determined that the precipitation point for NaPSS−CTAC complexes at moderate salt occurs at [r] ∼ 0.7. Small-angle X-ray scattering (SAXS) experiments are performed on insoluble complexes, obtained roughly for 0.7 < [r] < 1.40. To extract the impact of electrostatic interactions on structure, both types of scattering experiment were conducted at a series of moderate ionic strengths.

Experimental Section

Materials. A NaPSS standard (Polysciences, Inc.), CTAC (Aldrich) (also known as hexadecyltrimethylammonium chloride), deuterium oxide (Aldrich), and sodium chloride (Mallinckrodt) were all used as received. The standard had a weight-average molecular weight of 100 000 g/mol and a polydispersity 1.10 and was used for SANS. A polydisperse NaPSS sample (Aldrich, M_w ∼ 70 000 g/mol, polydispersity 3−5) was used in most SAXS experiments. It was verified that molecular weight and polydispersity, at least within the moderate ranges examined in these studies, have little effect on precipitation point or insoluble complex structures. The standard sample was sulfonated after anionic polymerization of styrene, while the polydisperse sample was prepared by radical polymerization of sulfonated monomer. The different preparations lead to slightly different levels of sulfonation: 90% for the former and 100% for the latter.

A more monodisperse polymer sample was necessary for the neutron experiments because we were interested in the question of how many micelles bind per chain. If there is strong polydispersity in length, then this question cannot be addressed. Ideally, we would have liked to work with 100% sulfonated monodisperse samples, but unfortunately such samples are not available.

Small-Angle X-ray Scattering. SAXS measurements were performed on a Rigaku RU-H3R rotating anode diffractometer equipped with an Osmic multilayer focusing optic and an evacuated Statton-type scattering camera (Cu Kα radiation; detector distance 460 mm). The scattering vector q ranged from 0.698 to 6.25 nm^{-1}. Patterns were acquired on Fuji ST-VA image plates and read with a Fuji BAS-2500 image plate scanner.

X-ray samples were prepared by mixing a 4.85 mM (based on monomer) NaPSS precursor solution containing 10, 100, and 200 mM NaCl with a 25 wt % solution of CTAC such that 0.7 < [r] < 1.40 was achieved. The concentrated surfactant solution was always, with thorough mixing, added to the polymer solution. A white precipitate quickly appeared, and this precipitate and its supernatant were equilibrated for at least 24 h; a few samples were equilibrated for 1 month to verify constancy and equilibration of structure. After equilibration, the precipitate was isolated by centrifugation and placed in a Teflon sample holder along with a portion of the supernatant. To prevent evaporation, samples in the holder were sealed between thin Mylar sheets.

Small-Angle Neutron Scattering. We chose to use small-angle neutron scattering (SANS) to investigate the structure of the soluble polyelectrolyte−surfactant complexes because this technique offers the unique possibility to vary the scattering contrast between different components of a mixture by selectively deuterating the solvent or the components. In our case, we used D_2O as a solvent which increases the overall contrast between the solvent and the surfactant, allowing us to elucidate the shape and size of the surfactant micelles.

SANS was conducted at the SAD beamline of Argonne National Laboratory using a short path length time-of-flight (TOF) instrument operated in conjunction with an intense pulsed source, which provided neutrons, after passage through the cold moderator, of wavelengths 0.9−14 Å. The practical range of q was 0.015−0.12 $Å^{-1}$. A full description of the beamline is provided elsewhere.[42] Solutions were examined in disk-shaped quartz cells of path length of 2 mm, and absolute scattered intensities were obtained from the 20 × 20 × 3.2 cm detector after calibration with H_2O and a cadmium reference.[43] Subtracting scattering background for both solvent and sample cells, and making adjustment for detector sensitivity, absolute scattering intensity is reported as $I(q)$ (cm^{-1}), the coherent scattering probability per unit solid angle divided by sample path length.

SANS samples were prepared in the same manner as X-ray samples, except the solvent was D_2O and polyelectrolyte concentrations were higher (12.1 or 24.25 mM). Again, NaCl was present at 10, 100, or 200 mM. Relevant concentrations of NaPSS and CTAC for each mixed sample are listed in Tables 1–3; mixing led to 0.1 ≤ [r] ≤ 0.66. No attempt was made to use contrast matching to extract the scattering contribution of the polyelectrolyte, though it is estimated to be minor.

Neutron Scattering Fitting Procedures. The scattering intensity for a suspension of uniform particles can be written

$$I(q) = n(\rho(r) - \rho_s)^2 V^2 P(q)\, S(q) \quad (1)$$

where n is the particle number density, $\rho(r)$ and ρ_s are the scattering length densities for particle and solvent, respectively, V is the

particle volume, $P(q)$ is the single particle form factor, and $S(q)$ is the interparticle structure factor. For very dilute particles, such as most of the complexes of this study, $S(q)$ can be set to unity. It was first shown that, for dense micelles such as CTAC, the prefactor $A = n(\rho(r) - \rho_s)^2V^2$ can be rewritten in a more explicit form.[44] For a system of dilute particles, such as a necklace of spherical surfactant micelles, the scattering intensity distribution $I(q)$ can be written as[7]

$$I(q) = n\nu(b_m - V_m\rho_s)^2P(q) \quad (2)$$

where n is now the number density of surfactant molecules in solution, ν is the average number of surfactant molecules per micelle, b_m is the scattering length for surfactant, and V_m is the volume of a surfactant molecule. The following solvent scattering length density, surfactant molecular volume, and surfactant scattering length were used in all calculations: $\rho_s = 6.33 \times 10^{-6}$ Å^{-2}, $V_m = 542.69$ Å^3, $b_m = -2.38 \times 10^{-4}$ Å.[45] The surfactant molecular volume was calculated using the apparent molar volume for CTAC in aqueous solution ($V_{CTAC} = 532$ Å^3).[46] Assuming all surfactant molecules assemble into spherical micelles of uniform size, the form factor is represented by

$$P(q) = |F(q)|^2 = \left(\frac{3[\sin(qR) - qR\cos(qR)]}{(qR)^3}\right)^2 \quad (3)$$

where $F(q)$ is the scattering amplitude function and R is the micelle radius.

As [r] increases (the complexes remaining dilute), additional spherical micelles bind along a single NaPSS chain, leading to enhanced intra-aggregate interference due to micelle localization. At the range of salt concentration employed, the radius of gyration of a 100 000 g/mol NaPSS chain is ~110 Å as deduced from the measured diffusion coefficients[47] and the Zimm model prediction for good solvents $R_g = 0.203k_BT/\sqrt{6\eta D_{bulk}}$.[48] The separation between micelles on a single polymer chain cannot much exceed R_g. We account for micelle−micelle interference by adopting the model of two spheres separated by a distance, a. A system with two spheres in close proximity with surfaces separated by a distance, a, can be represented by

$$I(q) = (n\nu(b_m - V_m\rho_s)^2)|F(q)|^2 2\left[1 + \frac{\sin(qa)}{qa}\right] \quad (4)$$

where $F(q)$ remains that described for a single sphere (eq 3). Scattering from a mixture of chains with one and two micelles can be described by the expression

$$I(q) = (n\nu(b_m - V_m\rho_s)^2)|F(q)|^2 N\left[1 + \frac{2(N-1)}{N}\frac{\sin(qa)}{qa}\right] \quad (5)$$

where N is the average number of micelles per chain ($1 < N \leq 2$).

At higher surfactant concentrations, but with complexes still soluble, a spherical form factor clearly fails to fit scattering data, and here, much more satisfactory is a solid cylindrical form factor

$$P_c(q) = \int_0^{\pi/2}\left[\frac{2B_1(qR\sin\alpha)}{qR\sin\alpha}\frac{\sin((qL\cos\alpha)/2)}{(qL\cos\alpha)/2}\right]^2 \sin\alpha\, d\alpha \quad (6)$$

where $P_c(q)$ is an average over all cylinder orientation angles α, B_1 is the first-order Bessel function, and R and L are cylinder radius and length, respectively. The angular averaging in eq 6 must be performed numerically.[49] During the fitting of $P_c(q)$ to data, the possibility of multicylinder complexes produced by bridging chains was neglected.

A selection of previous SAXS and SANS experiments on polyelectrolyte−surfactant complexes uncovered a Bragg peak at relatively high q ($0.1 \leq q \geq 0.2$),[16,23,24,26,40,41] indicating tight packing of micelles. In our SANS experiments, this q range was inaccessible, and thus no comment can be made concerning short-range micelle order. We deem such short-range order doubtful, as the systems at hand were all soluble while those producing a Bragg peak have been all phase-separated. While there may be coexistence between soluble and precipitated complexes, it would be difficult to isolate their individual scattering contributions. Our SANS experiments were performed below the independently determined precipitation point for NaPSS−CTAC complexes.

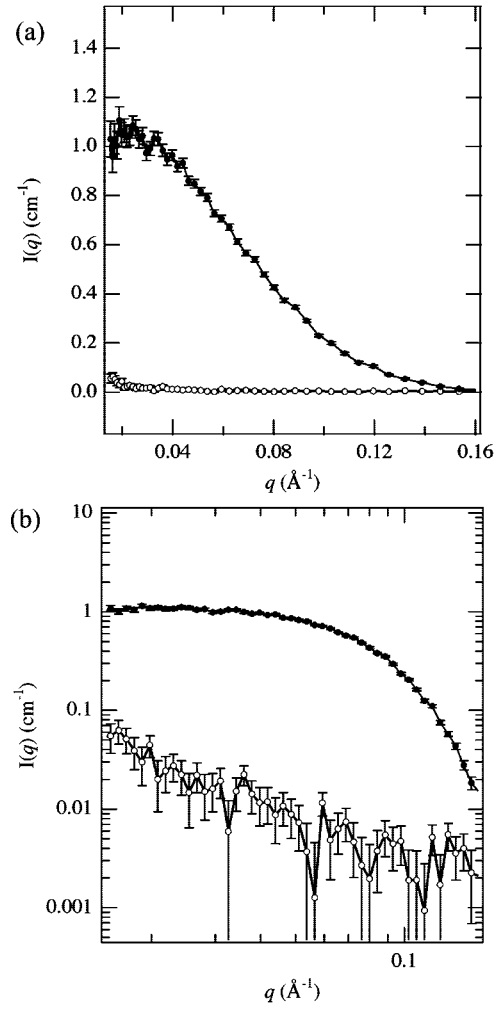

Figure 1. Comparison of absolute scattering intensity curves for 12.1 mM poly(styrenesulfonate) (○) and 12.1 mM CTAC (●) at 100 mM NaCl. Solid Lines are included for continuity and do not represent theoretical fits. A 12 h exposure time for PSS compared to 2 h for CTAC.

Results

SANS of NaPSS and CTAC. To highlight the difference in scattering contrast between NaPSS and CTAC, Figure 1 compares $I(q)$ for 12.1 mM NaPSS and 12.1 mM CTAC, both measured at 100 mM NaCl. Intensities for NaPSS and CTAC were accumulated for 12 and 2 h, respectively, and after accounting for this time difference, one discovers that CTAC scattering at low q exceeds that of NaPSS by almost 2 orders of magnitude. Subsequent SANS interpretations are thus based solely on structural models for surfactant. At 100 mM NaCl, the cmc of CTAC is ~0.1 mM, and as spherical micelles form above the cmc in pure CTAC solutions, the SANS data of Figure 1 fit a spherical form factor well using R as the only fitting parameter. Increasing NaCl concentration from 10 to 100 mM (data not shown), spherical form factor fits suggest slight growth of R, from 24.8 to 26.7 Å, and a modest rise in ν, from 96 to 120. Growth of charged micelles with increasing ionic strength is caused by the screening of head-group charges.[31]

SANS of NaPSS−CTAC Complexes. Figures 2–4 present SANS $I(q)$ data for NaPSS−CTAC complexes at 10, 100, and

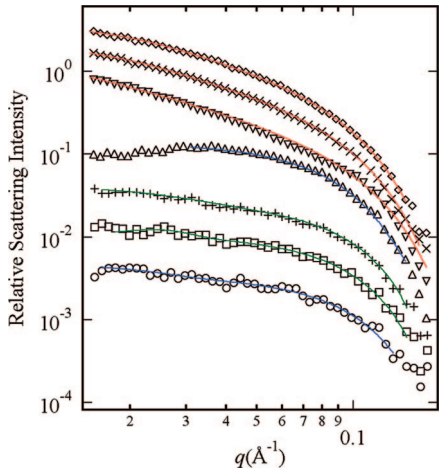

Figure 2. Small-angle neutron scattering curves for soluble poly(styrenesulfonate)/CTAC complexes in D_2O at 10 mM NaCl, for different values of [r]: 0.1 (○), 0.2 (□), 0.3 (+), 0.4 (Δ), 0.5 (▽), 0.6 (×), 0.66 (◇). Solid lines represent theoretical Fits. Fit functions are indicated by color (blue, eq 3; green, eq 5; red, eq 6). To avoid crowding, all curves have been shifted by multiplying the scattering intensity by 10^{-p}, where $p = 0$, 0.25, 0.5, 0.75, 1, 1.25, and 1.5, starting with the upper curve and working down.

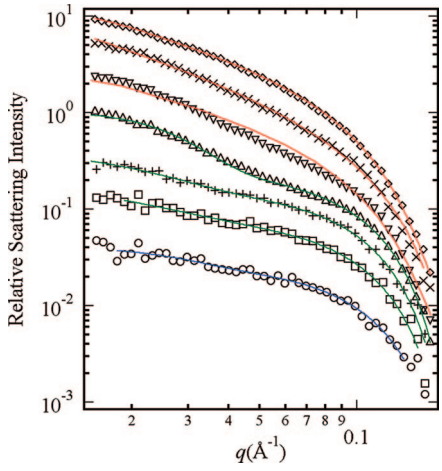

Figure 3. Small-angle neutron scattering curves for soluble poly(styrenesulfonate)/CTAC complexes in D_2O at 100 mM NaCl, for different values of [r]: 0.1 (○), 0.2 (□), 0.3 (+), 0.4 (Δ), 0.5 (▽), 0.6 (×), 0.66 (◇). Solid lines represent theoretical fits. Fit functions are indicated by color (blue, eq 3; green, eq 5; red, eq 6). To avoid crowding, all curves have been shifted by multiplying the scattering intensity by 10^{-p}, where $p = 0$, 0.25, 0.5, 0.75, 1, 1.25, and 1.5, starting with the upper curve and working down.

200 mM NaCl, respectively, as well as fits to the same data using eq 2 in conjunction with various form factors. To improve graphical clarity, the scattering data taken at different [r] (symbols) and the corresponding theoretical fit (color-coded solid lines: blue, eq 3; green, eq 5; red, eq 6) are shifted downward by a factor 10^{-p}, with larger p imposed for smaller values of [r] ($p = 0$, 0.25, 0.5, ...). Parameters returned by fitting are reported in Tables 1–3; in these tables and subsequent discussion, N_m is the average number of micelles bound per polymer chain. N_m is calculated from the measured aggregation number ($N_m = n/(\nu N_p)$), where N_p is the number density of PSS molecules, under the assumption that all surfactant molecules are present in bound micelles. A spherical form factor best fits $I(q)$ at low surfactant concentrations ([r] < 0.3), but as [r] increases, a broad peak not present in the spherical form factor emerges at low q. As seen from Figure 1, the same peak is not

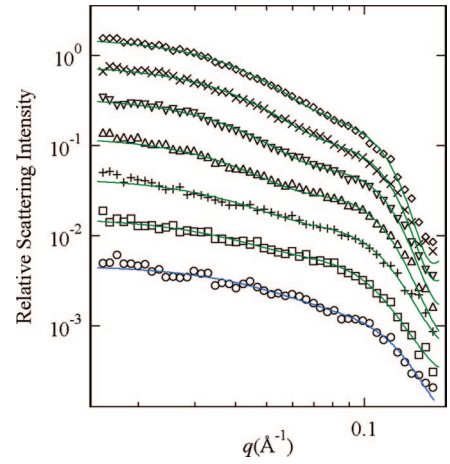

Figure 4. Small-angle neutron scattering curves for soluble poly(styrenesulfonate)/CTAC complexes in D_2O at 200 mM NaCl, for different values of [r]: 0.1 (○), 0.2 (□), 0.3 (+), 0.4 (Δ), 0.5 (▽), 0.6 (×), 0.66 (◇). Solid lines represent theoretical fits. Fit functions are indicated by color (blue, eq 3; green, eq 5). To avoid crowding, all curves have been shifted by multiplying the scattering intensity by 10^{-p}, where $p = 0$, 0.25, 0.5, 0.75, 1, 1.25, and 1.5, starting with the upper curve and working down.

seen for either NaPSS or CTAC alone. We attribute the peak to interference between spherical micelles attached along a single chain and model the interference using eq 5. Excellent fits to all data sets are thereby obtained, and as seen in Tables 1–3, the fits provide realistic values of ν and other parameters. The average aggregation number for each sample was calculated by two methods. The first, ν_a, was calculated from the amplitude that was returned from the model fit, as given in eq 2. The average aggregation number, ν_b, was also calculated on the basis of the radius measured in the model fit. Using the radius, it was possible to calculate the volume of the given micelle, and then by dividing by the volume of a single surfactant molecule, it was possible to calculate an aggregation number. This method assumes dense packing of molecules within the micelle and is likely to overestimate the aggregation number slightly. The resulting aggregation numbers can be found in Tables 1–3. Likewise, the number of micelles bound per polymer chain was calculated both from theory based on molar ratios (N_a) and from the model fit (N_b). The aggregation numbers calculated on the the basis of the average radius of the micelle are larger than expected when compared to theoretical values. If the average radius of the micelle is reduced by roughly 10%, the calculated values of ν_b and N_b are found to be in good agreement with the expected values. It is most likely that the slight increase in the observed radius is due to the presence of the polyelectrolyte bound to the surface of the micelle. As stated earlier, no attempt was made to use contrast matching to eliminate the contribution of the polyelectrolyte to the scattering data. It does not appear that the polyelectrolyte has significantly altered the scattering pattern but simply caused the micelle radius to be slightly exaggerated.

Interference between multiple micelles bound along single chains led to the appearance of a broad peak at low q. This was found to occur at intermediate values of [r] and was best fit with eq 5. The intermicelle spacing for the complexes can be found in Tables 1–3. In general, the average distance between micelles shrinks with increasing surfactant concentration. This trend can most clearly be seen in the 200 mM NaCl samples that maintain a spherical micellar phase throughout the soluble regime. Only minor differences in micelle spacing were observed with changes in ionic strength, with initial spacings being greatest at the lowest salt concentration.

The SANS data reveal that, on average, not more than about two spherical micelles bind to one NaPSS chain, a result deemed reasonable given the relatively small polyelectrolyte molecular weight; the coil's mean radius of gyration is not much bigger than the sum of diameters for two spherical micelles. The total number of negative charges on one polyelectrolyte is about 500, so ~5 spherical micelles could bind before the complex becomes overcharged. We see N_m approaching or exceeding 2 only when the salt concentration is high, a condition minimizing micelle−micelle electrostatic repulsion. In many cases, especially at low $[r]$, N_m is less than unity, revealing conditions under which many chains have no micelle attached. As will be described shortly, a cylindrical form factor best tracks data for soluble complexes at larger $[r]$, a feature compelling us to consider that $I(q)$ across the intermediate $[r]$ range ($0.3 < [r] < 0.5$) might alternatively be explained through coexistence of spherical and cylindrical micelles. Indeed, $[r] = 0.4$ at 10 mM NaCl fit neither the two-sphere model nor a cylindrical model. Equally, a fitting procedure combining the two form factors (spheres and cylinders) does not lead to realistic fits. We therefore applied a single-sphere fit to the high-q range of data that are reported in Figure 2 and Table 1.

At the highest $[r]$ values lying in the soluble regime ($0.50 < [r] < 0.66$), excellent fits are not achieved through any model incorporating spherical scattering entities, while good fits are possible by applying the form factor of a long cylinder. Although less physically reasonable, the form factor of an elongated ellipse of rotation works equally well. According to the cylinder fits, the elongated micelles have N_m just under unity; one can thus make a crude depiction of the average complex as one cylindrical surfactant micelle "wrapped" by a polyelectrolyte chain. The transition from the pearl necklace (few pearls) to wrapped cylinder is abrupt at low salt, where there is a sharp discontinuity of fitting parameters at this transition.

Discussion now turns to detailed trends in fit parameters for soluble complexes and how these trends reveal the evolution of complex structure with $[r]$. From the preceding paragraph, we hypothesize three regimes of soluble complex, associated with low ($[r] < 0.3$), moderate ($0.3 < [r] < 0.5$), and high ($0.5 < [r] < 0.66$) $[r]$. The presence and boundaries of these regimes vary somewhat with ionic strength. All trends must be considered in light of a key assumption made in the scattering analysis, namely, that all surfactant molecules reside in bound micelles. From surfactant electrode measurements (unpublished), we know that the free surfactant concentration is always below the critical micelle concentration, with increased free surfactant as the ionic strength is increased.[3]

At low and moderate $[r]$, R and ν remain essentially constant with increasing $[r]$. Thus, incremental additions of surfactant act mainly to increase N_m, leaving micelle properties unchanged. Bound micelles are approximately the same size as free micelles in pure CTAC solution—not nearly as small as first described by Almgren et al.[34] In various polyelectrolyte−surfactant systems there have been micelles observed that are smaller than,[34,50,51] on the same order[35,52] as, and larger than[53] micelles in polyelectrolyte-free surfactant solutions. As expected, at fixed low $[r]$, R and ν both rise slightly as ionic strength rises. This is likely due to the decrease in head-group repulsion between neighboring surfactant molecules with increasing ionic strength—the same trend expected for polymer-free surfactant solutions.

For samples made at 10 and 100 mM NaCl, cylindrical micelles abruptly appear as $[r]$ approaches the precipitation point; they are first noted at $[r] = 0.5$ at both 10 mM NaCl and 100 mM NaCl. In all instances, the cylindrical micelles are of roughly the same R, but L drops slightly with increasing $[r]$ at 10 mM. At 100 mM our fits indicate that the cylinder length exceeds 400 Å. Since our accessible lowest $q = 0.015$ Å^{-1}, we cannot easily distinguish between cylinders of length larger than $2\pi/q_{min} \approx 400$ Å. As expected, the cylindrical micelles have about the same radial dimension as the spherical micelles studied at lower $[r]$, and in both cases, this dimension is approximately consistent with the length sum of two extended CTAC molecules. The ratio of L to R is always greater than 5. As seen in Tables 1 and 2, as ionic strength increases from 10 to 100 mM, L seems to increase from ~200 Å to larger than 400 Å. At 100 mM it is likely that more than one polyelectrolyte chain is binding to a single cylindrical micelle since the micelle aggregation number exceeds the number of charges on a single polyelectrolyte.

Table 3. PSS/CTAC SANS Results (200 mM NaCl)

ratio	[PSS] (mM)	[CTAC] (mM)	R (Å)	a (Å)	ν_a	ν_b	N_a	N_b
0.1	12.04	1.204	25.1		105	121	0.48	0.44
0.2	11.98	2.396	24.9	78.0	96	119	1.04	0.84
0.3	10.52	3.16	24.2	71.7	101	109	1.49	1.38
0.4	10.08	4.03	24.8	72.0	110	117	1.82	1.71
0.5	9.68	4.84	25.9	66.4	125	134	2	1.87
0.6	9.31	5.58	26.8	63.0	141	148	2.13	2.03
0.66	9.1	6.0	27.4	61.9	151	158	2.19	2.09

A cylindrical phase in soluble polymer−surfactant complexes is a recent discovery. Although suggested by NMR and fluorescence experiments,[35,54] cylinders in polyelectrolyte−surfactant systems were first detected though scattering by Claesson and co-workers, who investigated complexes produced by the mixing of variably charged cationic copolymers of acrylamide and 3-(2-methylpropionamido)propyltrimethylammonium chloride (MAPTAC) with anionic sodium dodecyl sulfate.[26] Elliptical or cylindrical phases were found at all values of $[r]$ examined. Recently, Flood et al. imaged the soluble complexes of potassium oleate, and NaPSS by cryo-TEM, uncovering a structural transition between, as well as coexistence of, spherical and rodlike micelles.[55]

While the value of ν suggests that the cylindrical complexes are overcharged (more surfactant molecules than monomers within a single aggregate), the value of N_m is less than one. Thus, only about half the chains have bound to micelles, which are larger than the chains themselves, leaving the remaining chains to carry few or no surfactant micelles. It is difficult to discern whether there is ever coexistence of spherical and cylindrical micelles, but clearly cylindrical micelles dominate where this morphology was identified.

Increasing levels of NaCl screen the electrostatic interactions between NaPSS and CTAC as well as those between individual CTAC micelles bound along a single NaPSS chain. With weaker association to the polyelectrolyte chain and reduced repulsion between neighboring micelles, the transition from spherical to cylindrical micelle is pushed to higher $[r]$. Eventually, as seen at 200 mM NaCl, the cylindrical micelle regime disappears prior to precipitation.

SAXS of NaPSS−CTAC Complexes. Precipitated NaPSS−CTAC complexes, isolated for $0.72 < [r] < 1.4$, display nanoscale solid structural order assessed with SAXS. Under most conditions, increasing $[r]$ across this range leads to the following phase sequence: hexagonally close-packed cylinders (HCPC) → coexistence of HCPC and $Pm3n$ cubic → $Pm3n$ cubic. Complexes prepared at 200 mM NaCl, however, do not display the latter phase. Representative scattering patterns for the two pure phase structures, recorded for $[r] = 0.72$ and 1.4 in 100 mM NaCl, are displayed in Figure 5, each exhibiting only the narrow, characteristic peaks associated with a single phase structure. The respective peak ratios for HCPC and $Pm3n$ phases are $\sqrt{1}$, $\sqrt{3}$, $\sqrt{4}$, $\sqrt{7}$, $\sqrt{9}$ and $\sqrt{2}$, $\sqrt{4}$, $\sqrt{5}$, $\sqrt{6}$, $\sqrt{8}$, $\sqrt{10}$. [Note that the (200) reflection is the lowest order observed.] The $Pm3n$ phase, observed previously in similar

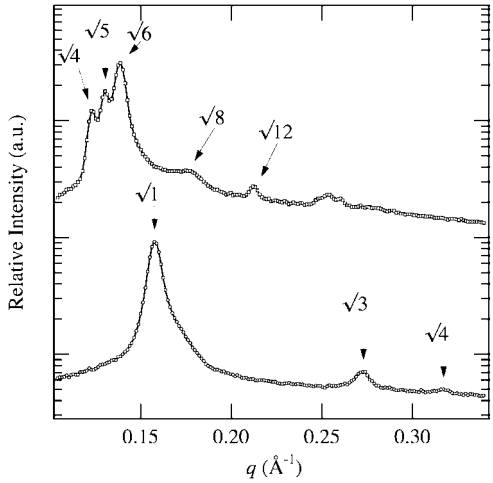

Figure 5. Angular-averaged small-angle X-ray scattering profiles for poly(styrenesulfonate)/CTAC complexes in 100 mM NaCl. Bottom trace ($r = 0.72$) displays scattering associated with a HCPC phase. Top trace ($r = 1.4$) displays scattering associated with a *Pm*3*n* cubic phase.

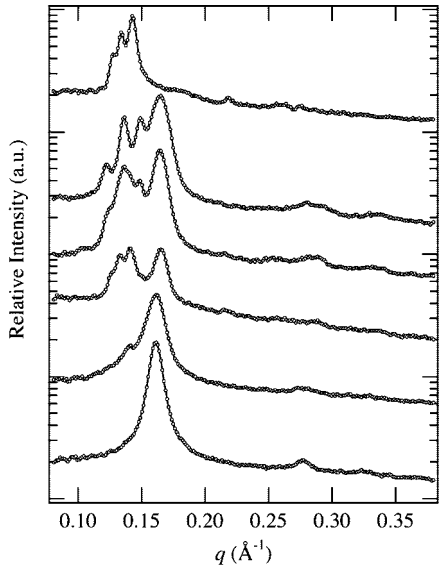

Figure 6. Angularly averaged SAXS profiles for PSS/CTAC insoluble complexes at 10 mM NaCl. Ratio, [*r*], of surfactant to polymer charge varies from bottom to top as 0.72, 0.78, 0.84, 1.03, 1.09, and 1.4.

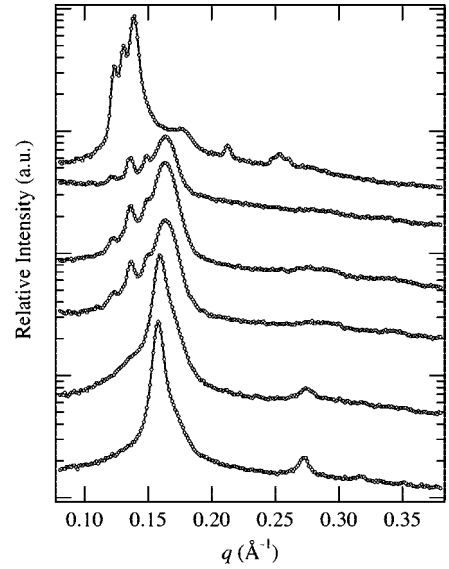

Figure 7. Angularly averaged SAXS profiles for PSS/CTAC insoluble complexes at 100 mM NaCl. [*r*] Values (from bottom to top): 0.72, 0.78, 0.84, 1.03, 1.09, and 1.4.

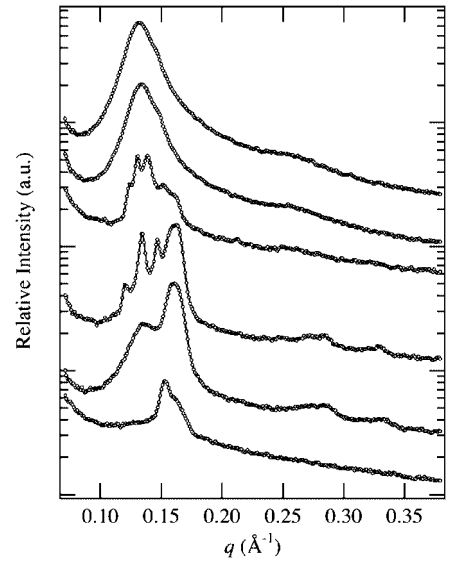

Figure 8. Angularly averaged SAXS profiles for PSS/CTAC insoluble complexes at 200 mM NaCl. [*r*] values (from bottom to top): 0.73, 0.85, 0.9, 1.0, 1.1, and 1.2.

condensed colloidal systems,[56,57] was theoretically described by Kamien et al.[58]

As shown in Figures 6 and 7, the [*r*] progression of phase structures for 10 and 100 mM NaCl are similar. Precipitation occurs at [*r*] $\sim$ 0.7, and at [*r*] = 0.72, a well-ordered HCPC morphology is found by SAXS. Very little precipitate is produced until [*r*] = 0.72, hindering identification of the phase morphology exactly at the point of precipitation, but there is no reason to expect a phase change over the narrow intervening [*r*] range. As [*r*] grows beyond 0.72, i.e., as more surfactant is added to a constant level of polyelectrolyte, increasingly greater masses of precipitate are observed, making isolation simpler. At [*r*] $\sim$ 0.8, HCPC begins to transform to *Pm*3*n* cubic, with coexistence of the two morphologies persisting up through [*r*] = 1.4−1.5, at which point the latter phase dominates.

Similar progressions have been seen previously, for example, in the complexes of NaPSS and CPC studied by Kogej et al.,[40,41] who varied [*r*] from 0.3 to 1.3; HCPC morphology was monitored at [*r*] greater than 1, but neither coexistence nor a *Pm*3*n* cubic morphology was observed. Interestingly, for poly(acrylic acid)−CTAC complexes, we have tracked an inverted progression of phases, with the initial *Pm*3*n* cubic morphology replaced at higher [*r*] by the HCPC morphology.[11]

The effect of ionic strength is most clearly seen by comparing Figure 8, which displays SAXS data for samples prepared at 200 mM NaCl, with Figures 6 and 7. The scattering profiles of Figure 8 possess fewer higher-order peaks, and these peaks are rather broad, indicating order over a limited length scale. The sharpest peaks are noted near [*r*] = 1.0, where coexistence of HCPC phase and *Pm*3*n* cubic phases is deduced. At [*r*] greater than 1.0, order is slowly lost, and the majority of the precipitate is observed to redissolve. From unpublished calorimetry data at 200 mM NaCl, we know that the cmc for free CTAC micelles lies little above the concentration of complex precipitation. The redissolution of polyelectrolyte−surfactant complexes in this

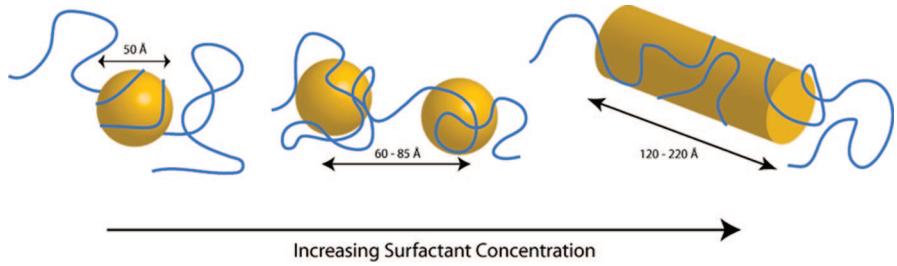

Figure 9. Depiction of soluble phase progression for PSS−CTAC system (not drawn to scale).

regime thus linked not only to weakened electrostatic interactions but also to charge reversal.[43]

Discussion

For NaPSS−CTAC complexes, the phase sequence under increasing [*r*] follows: disordered spherical phase (soluble) → disordered cylindrical phase (soluble) → HCPC (insoluble) → coexistence → *Pm*3*n* cubic (insoluble). This progression is nearly analogous to that followed by aqueous CTAC as surfactant concentration rises.[59] The exception is the replacement of the *Pm*3*n* cubic phase by the *Ia*3*d* cubic phase at high [*r*], as previously observed in several polyelectrolyte−surfactant complexes.[11,16,17] One may thus conclude that, although the interactions in polyelectrolyte−surfactant complexes differ somewhat from those among surfactant molecules in a concentrated surfactant solution, in both cases, the surfactant molecule spontaneous curvature determines overall structure (spherical vs cylindrical), the polyelectrolyte acting mainly as a cohesive material. We argued previously that the structures of polyelectrolyte−surfactant complexes emerge mainly from the competition between surfactant spontaneous curvature and surfactant packing constraints.[11]

The soluble structures observed at very low [*r*] in dilute solution have been observed previously in a number of scattering studies. These structures are also very similar to those seen in protein−surfactant and nonionic polymer−surfactant complexes[5,6,60,61] in which the polymer chain wraps around a spherical micelle or multiple spherical micelles. These results are in agreement with expectations. It is believed that the PSS−CTAC system follows the trend described in Figure 9.

To rationalize the formation mechanism of cylindrical micelles in our system, we consider two possibly complementary explanations. One is based on a thermodynamic model by Hansson that describes structures of polyelectrolyte−surfactant complexes.[37] The model predicts attraction between micelles that are bound to the same polyelectrolyte coils which leads to a solution of polyelectrolytes with tightly packed micelles in equilibrium with surfactant-free coils. The model considers only the possibility of spherical micelles. Apparently, packed tightly enough micelles could collapse into a single cylindrical micelle to explain our data. Also, by reducing the penalty of electrostatically unfavorable cylindrical regions through polyelectrolyte binding, the formation of cylinders is favored over spherical micelles as more surfactant binds.

To our knowledge, we are the first to identify a dilute polyelectrolyte−surfactant system that forms a soluble cylindrical phase. From fitting procedures the dimensions of the observed micelles are in line with those expected for CTAC micelles, with a diameter equivalent to the length of two CTAC molecules placed end to end. Structures similar to this had been previously theorized to exist but had not been identified conclusively through scattering or microscopic techniques. For example, Kasaikin and Zakharova depicted similar structures appearing in the soluble regime, prior to precipitation, of poly(acrylic acid)−CTAB complexation.[52] Though they only had ultracentrifuge data to rely on, they predicted these structures on the basis of the size of the dilute complexes.

Conclusions

The structural evolution as charged surfactant is titrated into oppositely charged polyelectrolyte has been followed by SANS and SAXS, the former in the soluble complex domain and the latter in the insoluble complex domain. The observed progression of structures for NaPSS−CTAC complexes can be explained reasonably well in terms of the polyelectrolyte's impact on micelle spontaneous curvature and micelle packing: the polyelectrolyte binds the micelles together, raising their density, and inserts into micelles, altering their spontaneous curvature. The major new structural feature is a window of [*r*] in the soluble domain in which spherical micelles yield to cylindrical micelles. One can imagine that, at the precipitation point, these cylindrical micelles organize to form an ordered cylinder phase. The significant hydrophobicity of NaPSS, resulting in a nonelectrostatic attraction between NaPSS and CTAC, reduces the precipitation point significantly below a bulk stoichiometric balance of charge to [*r*] $\sim$ 0.7. By our assumption that surfactants are fully incorporated into bound micelles, the bulk charge balance, reflected in [*r*], is identical to the local charge balance within a single soluble complex. Excepting the appearance of soluble cylindrical micelles, the overall phase progression is similar to that of the pure surfactant except with structural transitions shifted to lower surfactant concentration. The concentration of added salt affects the electrostatic interactions, both between polyelectrolyte and surfactant micelle (attractive) and between surfactant micelles bound closely to each other along a single polyelectrolyte chain (repulsive). Both electrostatic interactions are important, modifying the phase progress and even eliminating phases in a predictable manner. Most importantly, at high salt, the weakened attraction between components causes a loss of order in the insoluble precipitate formed at high [*r*].

Acknowledgment. We acknowledge support of the Center for Research on Polymers at the University of Massachusetts Amherst (CUMIRP Cluster G). Some of the results shown in this report are derived from work performed at Argonne National Laboratory. Argonne is operated by UChicago Argonne, LLC, for the U.S. Department of Energy under Contract DE-AC02-06CH11357. We especially thank Jyotsana Lal for her help with the small-angle neutron scattering experiments. Facilities of the University of Massachusetts NSF-funded Materials Research Science and Engineering Center (DMR-0213695) were also employed in this study.

References and Notes

(1) Kogej, K.; Skerjanc, J. *Langmuir* **1999**, *15*, 4251–4258.
(2) Kogej, K.; Skerjanc, J. *Acta Chim. Slov.* **1998**, *45*, 443–453.
(3) Hayakawa, K.; Kwak, J. C. T. *J. Phys. Chem.* **1982**, *86*, 3866–3870.
(4) Hayakawa, K.; Kwak, J. C. T. *J. Phys. Chem.* **1983**, *87*, 506–509.
(5) Cabane, B.; Duplessix, R. *J. Phys. (Paris)* **1982**, *43*, 1529–1542.
(6) Cabane, B.; Duplessix, R. *Colloids Surf.* **1985**, *13*, 19–33.

(7) Guo, X. H.; Zhao, N. M.; Chen, S. H.; Teixeira, J. *Biopolymers* **1990**, *29*, 335–346.
(8) Ilekti, P.; Piculell, L.; Tournilhac, F.; Cabane, B. *J. Phys. Chem. B* **1998**, *102*, 344–351.
(9) Zhou, S. Q.; Hu, H. B.; Burger, C.; Chu, B. *Macromolecules* **2001**, *34*, 1772–1778.
(10) Zhou, S. Q.; Yeh, F. J.; Burger, C.; Chu, B. *J. Phys. Chem. B* **1999**, *103*, 2107–2112.
(11) Leonard, M. J.; Strey, H. H. *Macromolecules* **2003**, *36*, 9549–9558.
(12) Sokolov, E. L.; Yeh, F. J.; Khokhlov, A.; Chu, B. *Langmuir* **1996**, *12*, 6229–6234.
(13) Zhou, S. Q.; Yeh, F. J.; Burger, C.; Chu, B. *J. Polym. Sci., Part B: Polym. Phys.* **1999**, *37*, 2165–2172.
(14) Zhou, S. Q.; Yeh, F. J.; Burger, C.; Chu, B. *Scattering Polym.* **2000**, *739*, 244–260.
(15) Zhou, S. Q.; Yeh, F. J.; Burger, C.; Hu, H. B.; Liu, T. B.; Chu, B. *Polym. Adv. Technol.* **2000**, *11*, 235–241.
(16) Kogej, K.; Theunissen, E.; Reynaers, H. *Langmuir* **2002**, *18*, 8799–8805.
(17) Zhou, S.; Burger, C.; Yeh, F.; Chu, B. *Macromolecules* **1998**, *31*, 8157–8163.
(18) Kevelam, J.; Breemen, J. F. L. v.; Blokzijl, W.; Engberts, J. B. F. N. *Langmuir* **1996**, *12*, 4709–4717.
(19) Bai, G.; Wang, Y.; Yan, H. *J. Phys. Chem. B* **2002**, *106*, 2153–2159.
(20) Kogej, K.; Evmenenko, G.; Theunissen, E.; Berghmans, H.; Reynaers, H. *Langmuir* **2001**, *17*, 3175–3184.
(21) Kogej, K.; Theunissen, E.; Reynaers, H. *Langmuir* **2002**, *18*, 8799–8805.
(22) Kogej, K.; Evmenenko, G.; Theunissen, E.; Skerjanc, J.; Berghmans, H.; Reynaers, H.; Bras, W. *Macromol. Rapid Commun.* **2000**, *21*, 1226–1233.
(23) Lee, L.-T. *Curr. Opin. Colloid Interface Sci.* **1999**, *4*, 205–213.
(24) Claesson, P. M.; Bergstrom, M.; Dedinaite, A.; Kjellin, M.; Legrand, J. F.; Grillo, I. *J. Phys. Chem. B* **2000**, *104*, 11689–11694.
(25) Svensson, A.; Piculell, L.; Karlsson, L.; Cabane, B.; Jonsson, B. *J. Phys. Chem. B* **2003**, *107*, 8119–8130.
(26) Bergstrom, L. M.; Kjellin, U. R. M.; Claesson, P. M.; Grillo, I. *J. Phys. Chem. B* **2004**, *108*, 1874–1881.
(27) Israelachvili, J. N. *Intermolecular and Surface Forces*; Academic Press: London, 1992.
(28) Vollmer, D.; Vollmer, J. *Eur. Phys. J. E* **2001**, *4*, 153–159.
(29) Palazzo, G.; Carbone, L.; Colafemmina, G.; Angelieo, R.; Ceglie, A.; Giustini, M. *Phys. Chem. Chem. Phys.* **2004**, *6*, 1423–1429.
(30) Imae, T.; Kamiya, R.; Ikeda, S. *J. Colloid Interface Sci.* **1985**, *108*, 215–225.
(31) Yuet, P. K. *Langmuir* **2004**, *20*, 7960–7971.
(32) Khokhlov, A. R.; Kramarenko, E. Y.; Makhaeva, E. E.; Starodubtsev, S. G. *Macromolecules* **1992**, *25*, 4779–4783.
(33) Warnheim, T.; Jonsson, A. *J. Colloid Interface Sci.* **1988**, *125*, 627–633.
(34) Almgren, M.; Hansson, P.; Mukhtar, E.; Vanstam, J. *Langmuir* **1992**, *8*, 2405–2412.
(35) Hansson, P.; Almgren, M. *Langmuir* **1994**, *10*, 2115–2124.
(36) Hansson, P.; Almgren, M. *J. Phys. Chem. B* **2000**, *104*, 1137–1140.
(37) Hansson, P. *Langmuir* **2001**, *17*, 4167–4180.
(38) Fundin, J.; Brown, W. *Macromolecules* **1994**, *27*, 5024–5031.
(39) Fundin, J.; Hansson, P.; Brown, W.; Lidegran, I. *Macromolecules* **1997**, *30*, 1118–1126.
(40) Kogej, K.; Evmenenko, G.; Theunissen, E.; Berghmans, H.; Reynaers, H. *Langmuir* **2001**, *17*, 3175–3184.
(41) Kogej, K.; Evmenenko, G.; Theunissen, E.; Skerjanc, J.; Berghmans, H.; Reynaers, H.; Bras, W. *Macromol. Rapid Commun.* **2000**, *21*, 1226–1233.
(42) Thiyagarajan, P.; Epperson, J. E.; Crawford, R. K.; Carpenter, J. M.; Klippert, T. E.; Wozniak, D. G. *J. Appl. Crystallogr.* **1997**, *30*, 280–293.
(43) Wignall, G. D.; Bates, F. S. *J. Appl. Crystallogr.* **1987**, *20*, 28–40.
(44) Chen, S.-H.; Sheu, E. Y. *Macromol. Chem., Macromol. Symp.* **1988**, *15*, 275–294.
(45) Munter, A. Scattering Length Calculator. http://www.ncnr.nist.gov/resources/sldcalc.html (6/15/01).
(46) Simanenko, Y. S.; Popov, A. F.; Prokop'eva, T. M.; Karpichev, E. A.; Belousova, I. A.; Savelova, V. A. *Theor. Exp. Chem.* **2002**, *38*, 242–249.
(47) Wang, L.; Yu, H. *Macromolecules* **1988**, *21*, 3498–3501.
(48) Doi, M.; Edwards, S. F. *The Theory of Polymer Dynamics*; Oxford University Press: New York, 1986.
(49) Pedersen, J. S. *J. Appl. Crystallogr.* **2000**, *33*, 637–640.
(50) Fundin, J.; Hansson, P.; Brown, W.; Lidegran, I. *Macromolecules* **1997**, *30*, 1118–1126.
(51) Hansson, P.; Almgren, M. *J. Phys. Chem. B* **2000**, *104*, 1137–1140.
(52) Kasaikin, V. A.; Zakharova, J. A. *Colloids Surf., A* **1999**, *147*, 107–114.
(53) Li, Y.; Xu, R.; Couderc, S.; Bloor, D. M.; Warr, J.; Penfold, J.; Holzwarth, J. F.; Wyn-Jones, E. *Langmuir* **2001**, *17*, 5657–5665.
(54) Nakamura, K.; Yamanaka, K.; Shikata, T. *Langmuir* **2003**, *19*, 8654–8660.
(55) Flood, C.; Dreiss, C. A.; Croce, V.; Cosgrove, T. *Langmuir* **2005**, *21*, 7646–7652.
(56) Fontell, K. *Colloid Polym. Sci.* **1990**, *268*, 264–285.
(57) Lindblom, G.; Rilfors, L. *Biochim. Biophys. Acta* **1989**, *988*, 221–256.
(58) Ziherl, P.; Kamien, R. D. *Phys. Rev. Lett.* **2000**, *85*, 3528–3531.
(59) Auvray, X.; Petipas, C.; Anthore, R.; Rico, I.; Lattes, A. *J. Phys. Chem.* **1989**, *93*, 7458–7464.
(60) Guo, X. H.; Zhao, N. M.; Chen, S.-H.; Teixeira, J. *Biopolymers* **1990**, *29*, 335–346.
(61) Chen, S.-H.; Teixeira, J. *Phys. Rev. Lett.* **1986**, *57*, 2583–2586.

MA071634U